7th International Conference on Contact Mechanics and Wear of Rail/Wheel Systems
(CM2006), Brisbane, Australia, September 24-26, 2006

WAGON-TRACK MODELLING AND PARAMETRIC STUDY ON RAIL CORRUGATION INITIATION DUE TO WHEEL STICK-SLIP PROCESS ON CURVED TRACK

Y. Q. SUN* and S. SIMSON

Centre for Railway Engineering, Central Queensland University
Rockhampton, QLD 4702, Australia
Tel: +61 7-4930-9287; Fax: +61 7-4930-6984

Email: y.q.sun@cqu.edu.au and s.simson@cqu.edu.au

ABSTRACT

For the investigation of rail corrugation formation due to the wheel stick-slip process on curved tracks, a nonlinear wagon-track model is presented in this paper. In this model, the wagon movements were described using up to 78 degrees of freedom (Dofs). The two wheels in a wheelset are coupled through the stiffness coefficients corresponding to the natural torsional and bending modes of wheelset. The track is considered as a discretely supported distributed-parameter track modelling with one layer. In the wheel-rail interface, before the creep saturation point $\mu_s N_c$ (μ_s - static wheel-rail friction coefficient, N_c - normal force), the creep forces and moments are calculated using Kalker's linear creep theory. After that point, the wheel slides on the rail and the friction force will be $\mu_k N_c$ (μ_k - kinetic friction coefficient). Simulations show that the frequency of wheel stick-slip process is composed of a basic frequency, which matches the sleeper-passing frequency and the combined torsional and bending frequency of the wheelset, forming the wavelength of rail corrugation at different situations. Generally, the wheel stick-slip process on the high rail oscillates at the basic frequency while the dominant frequency on the low rail is double basic frequency. The effects of the curved track parameters, the wheel-rail friction characteristics and the wheel-rail profiles on wheel stick-slip process were investigated.

1 INTRODUCTION

The rail corrugations are of great practical concerns to the railway industry. Substantial savings could be made if rail corrugations could be prevented rather than simply treated. For the last 100 years, many theoretical and experimental studies have been conducted to explain the rail corrugation formations. Generally, the rail corrugation initiations have been described due to the wagon-track system resonances [1] ~ [14] (wheel-rail dynamic load P_2 resonance, flexural and/or torsional resonances of wheelset, sleeper resonance, track pinned-pinned resonances, etc.) and the wheel stick-slip process on the rail [15] ~ [25]. However, the theories on rail corrugations have not explained the formation mechanism perfectly and no perfect countermeasures have been established so far [26].

The widely accepted explanation of the rail corrugations due to the wheel stick-slip process is that when the creepage at wheel-rail contact patch is large enough to overcome the wheel-rail interface's ability to accommodate it, the wheel will skid on the rail. The reduction of friction force between wheel and rail during wheel sliding sometimes triggers a spring resonance response, reducing forces and making wheel stick to rail again. The wheel stick-slip process will cause the more or less periodic irregularities on the running surfaces of rails, which are often visible to the naked eye, and cause the high dynamic loads between wheels and rails, deteriorating the track and vehicle components and resulting in the high noise.

In order to comprehensively understand the characteristics of rail corrugation formation due to the wheel stick-slip process, a detailed nonlinear wagon-track model has been developed. In this model, the wagon was modelled using up to 78 Dofs, including one wagon car body, two bolsters, four sideframes and four wheelsets. Innovatively, the two wheels in a wheelset were coupled through the stiffness coefficients corresponding to the natural torsional and bending modes of wheelset. The higher order bending modes of the axle were not considered by the model. Wheel lateral flexing modes seen in wheel squeal were also not considered. A conventional ballasted track was considered. The track modelling is simplified as one layer structure – rail beams supported by discrete spring and damper elements representing the viscoelasticity of pad, sleeper, ballast and subgrade. For wheel-rail interface modelling, before the creep saturation, Johnson-Vermeulen's theory [27] was applied for the relationship between creepage and creep force. After the creep saturation, wheel sliding was considered.
It has been observed [28] that the rail corrugation due to wheel stick-slip process frequently occurs on the curved track, and is often worse on the low rail. The

current study is focusing on the application of wagon-track modelling on the curved tracks. Also, the parametric study of wagon-track modelling on rail corrugation has been carried out. The effects of the curved track parameters such as curvature and cant, the friction characteristics at wheel-rail interface, and the wheel-rail profiles on wheel stick-slip process were investigated.

2 WAGON-TRACK SYSTEM MODELLING

The wagon-track system modelling for rail corrugation initiation includes three subsystems, namely, the wagon subsystem, the track subsystem and the wheel-rail interface subsystem. Their dynamic characteristics are briefly described in this section.

2.1 Wagon subsystem

Wagon subsystem includes one wagon car body, two bolsters, four sideframes and four wheelsets. The wagon car body rests on two bolsters through two centre bowls and four constant-contact side bearings on bolsters. Each centre bowl is modelled as four point contacts having the spring and friction elements. The friction elements act in the longitudinal and lateral directions. The constant-contact side bearing is simplified as spring elements in the vertical direction. The bolster is supported by the secondary suspensions. The sideframe is an intermediate structure that provides seating for the secondary suspension element and connects to the wheelsets through the primary suspension elements and wheel bearing. Two wheels on a wheelset are coupled through the stiffness coefficients corresponding to the natural torsional and bending modes of wheelset. Nonlinear characteristics of interactions between wagon car body and bolsters, bolster and sideframes, and sideframes and wheelset are fully considered.

Except for the secondary and the primary suspension elements, all the other components of the wagon are considered as rigid bodies with masses and mass inertia moments along the three Cartesian coordinate directions. All movements of the wagon subsystem are taken into account. The total Dofs required to describe the longitudinal, lateral and the vertical displacements and rotations of the full wagon are listed in Table 1 in which u, v, w are the linear displacements and ϕ_x, ϕ_y, ϕ_z are the rotations about X, Y and Z axes respectively. As shown, there are 78 Dofs required to fully define the wagon dynamics.

The equations of dynamic equilibrium can be written using multi-body mechanics method as shown below:

$$\mathrm{M_W}\ddot{d}_W + \mathrm{C_W}\dot{d}_W + \mathrm{K_W}d_W = F_{WT} \qquad (1)$$

Table 1. Degrees of freedom of wagon

Components	u	v	w	ϕ_x	ϕ_y	ϕ_z
Wagon car body	×	×	×	×	×	×
Bolster	×	×	×	×	×	×
Sideframe	×	×	×	×	×	×
Wheelset	×	×	×			
Wheel				×	×	×
Total Dofs	1×6+2×6+4×6+4×3+8×3 = 78					

where $\mathrm{M_W}$, $\mathrm{C_W}$ and $\mathrm{K_W}$ are the mass, damping and stiffness matrices of the wagon subsystem. These matrices are 78×78 respectively. d_W is the displacement vector of the wagon subsystem, and F_{WT} is the interface force vector between the wagon and the track subsystems consisting of the wheel-rail normal contact forces, tangent creep forces and creep moments about normal direction in the wheel-rail contact plane.

2.2 Track subsystem

The track subsystem is considered as the discretely supported distributed-parameter track modelling with one layer. In the model, all the track components beneath rails used in the conventional ballasted heavy haul track structure are simplified as the spring and damper elements, which discretely support the rails at an interval of sleeper spacing.

The lateral and the vertical bending and shear deformations of the rail beam are described using Timoshenko beam theory extended by considering the torque of the rail beam. Thus, five Dofs at any point along the longitudinal neutral axis of the rail beam, namely, lateral and vertical displacements and rotations about the lateral (Y) and vertical (Z) axes and the torsional rotation about the longitudinal (X) axis are used in the formulation of the rail beam. For simplicity, the dynamic equilibrium equations of the rail beam has been expanded using Fourier series in the longitudinal (X) direction by assigning equal number of terms (n_m, also known as the number of modes of the rail beam) for both the linear displacements and the angular rotations. The governing equations of dynamic equilibrium for the track are expressed in the following matrix form:

$$\mathrm{M_T}\ddot{d}_T + \mathrm{C_T}\dot{d}_T + \mathrm{K_T}d_T = \tilde{F}_{WT} \qquad (2)$$

in which $\mathrm{M_T}$, $\mathrm{C_T}$ and $\mathrm{K_T}$ (each of size $10n_m \times 10n_m$) are the mass, damping and stiffness matrices of the track subsystem. The vector d_T contains displacement of the track subsystem which includes the modal and physical displacements, and $\tilde{F}_{WT}$ is the combined interface force vector between the wagon and the track subsystems.

2.3 Wheel-rail interface subsystem

Under rolling contact the wheel and the rail produce the contact forces in the normal direction on the wheel-rail contact plane. In addition, the creep forces are generated in the longitudinal and the lateral directions tangential to the contacting plane, and the creep moment about the normal direction. In this paper, the normal contact force due to the wheel-rail rolling contact is determined using Hertz contact theory.

The creep forces are determined according to the Figure 1, which shows the relationship between the creep force and the creepage. Generally, when a wagon with three-piece bogies is negotiating a curve, the wheel creep forces increase as the curve radius decreases. When the creep force on a wheel reaches the creep saturation value, the wheel begins to slip on the rail because the creep force overcomes the wheel-rail interface's ability to accommodate it, as shown in Figure 1. The wheel slip results in the reduction of friction force between the wheel and the rail, causing release of the restrained wheelset and rail flexibilities. The wheelset and rail stiffness forces reduce with release allowing the wheel contact to return to the stick part of the creep force creepage curve. Therefore, the periodic wheel stick-slip process is imitated by the model.

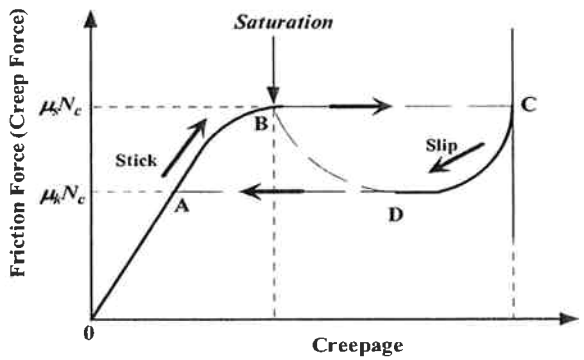

Figure 1. Wheel-rail stick-slip cycle

In Figure 1, before the creep saturation point, the wheel is kept stuck on the rail; at the saturation point, the creep force reaches the maximum value $\mu_s N_c$; after the saturation point, the wheel slides on the rail and the friction force will be $\mu_k N_c$. Some static and kinetic friction coefficients for the steel and steel contact at the dry condition are listed in Table 2

Table 2. Friction coefficients

μ_s	0.15	0.6	0.74
μ_k	0.09	0.4	0.57

Before the creep saturation point, the creep forces and moments are calculated using Kalker's linear creep theory [27]. The creep forces and moments are usually determined without due consideration to the velocities of rail, in other word, considering the track as rigid. In this wagon-track modelling, the velocities of the rail in the lateral and spin directions are included in these calculations of creepage. As Kalker's linear theory best defines the creep forces only when the creepages are very small, Johnson-Vermeulen's approach [27] is used to further modify the creep forces.

2.4 Selection of a wagon-track system

For the modelling of the wagon-track system, FORTRAN code has been written to the simulation calculation. A modified Newmark-β integration scheme was used to solve the differential equations of motions of wagon-track system.

A typical coal wagon and a curved track section with concrete sleepers at 0.685m sleeper spacing has been selected for the case study. Detailed parameters of the wagon-track system are given in Appendix Table-1. In the simulation, a new wheel-rail profile is selected. The contact parameters required for the simulation are calculated using VAMPIRE software and provided as "look-up" tables. Graphical representation of the contact parameters – in particular the radius of curvature of wheel profile at the contact point is shown in Figure 2.

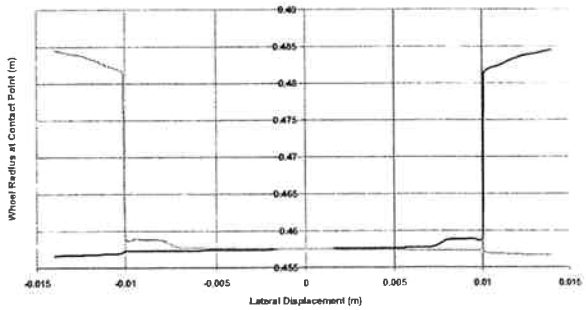

Figure 2. Radius of curvature of a wheel-rail profile

3. SIMULATION RESULT DISCUSION

A case simulation is carried out on the 240m radius curved track (transition length is 50m and curve length is 100m) with the cant of 65mm on narrow gauge track (1065mm). Wagon speed is 50km/h. The static and kinetic friction coefficients between wheel and rail are selected to be 0.3 and 0.22 respectively. The outputs are the creep force saturation values which are the product of static friction coefficient multiplied by normal force ($\mu_s N_c$) and divided by static wheel load, and the creep force factor which is the resultant creep force divided by static wheel load.

Generally, when a wagon with three-piece bogies is negotiating a curve, the creep forces on the two wheels of leading wheelset are larger than those of trailing wheelset, reflecting the influence of bogie rotation

resistance on the bogie lozenge which is opposed for the two wheelsets. Figure 3 (a) and (b) show the creep force saturation values and the creep force factor on both high and low rails generated on leading and trailing wheelsets respectively. In Figure 3 (a) and (b), the simulation shows that the creep forces on leading wheelset reach the creep saturation value whilst the trailing wheelset does not reach the saturation.

From Figure 3 (a), it can be seen that wheel stick-slip processes happen on the both wheels of leading wheelset over the whole curve. Although the stick-slip process does not occur on the either wheel of trailing wheelsets, the wheel-rail creep forces oscillate due to the effect of wheel stick-slip processes on leading wheelset as shown in Figure 3 (b). Figure 3 (c) and (d) clearly show the wheel stick-slip processes on both high and low rails over 4m. From Figure 3 (c), it can be seen that the creep force on the high rail oscillates at a basic frequency of 23.5Hz, which is found to be close to the sleeper-passing frequency (50/3.6/0.685 = 20.3Hz) and approximately one third of wheelset torsional frequency of 75.6Hz as given in Table-1. From Figure 3 (d), it can be seen that the creep force on the low rail vibrates at double the frequency to that of the high rail. Correspondingly, the wavelength of wheel stick-slip process on the high rail is about 0.62m whilst the wavelength on the low rail is about 0.31m.

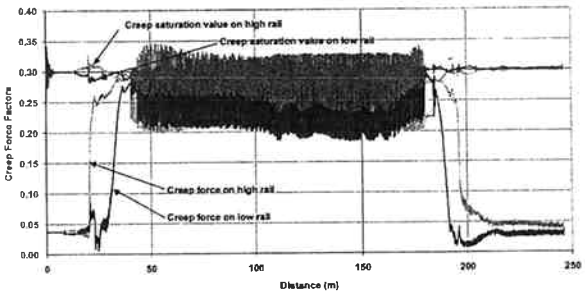

(a) On Leading Wheelset

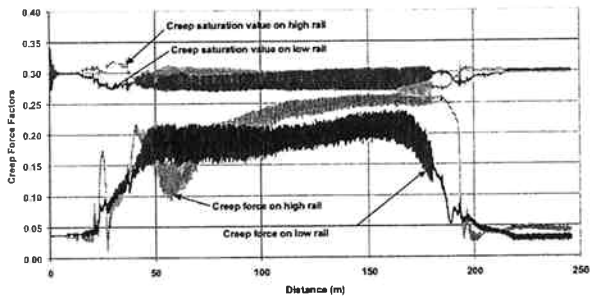

(b) On Trailing Wheelset

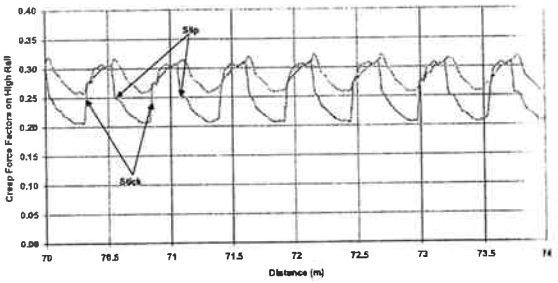

(c) Zoom of High Rail in (a)

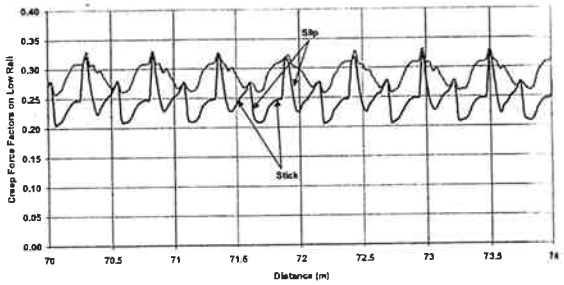

(d) Zoom of Low Rail in (a)

Figure 3. Creep Forces and Saturation Values

4. PARAMETRIC STUDIES

4.1 Effect of track curvature

In order to examine the effect of track curvature on wheel stick-slip process, the simulation is carried out on the track with 420m radius. The other track parameters – transition length, curve length and cant are the same as those with 240m radius. Wagon speed is 50 km/h. The new wheel-rail profile is used. The static and kinetic friction coefficients between the wheel and the rail are selected to be 0.3 and 0.22 respectively. Figure 4 shows the creep force saturation values and the creep force factors on both high and low rails at the leading wheelset location in this situation.

The simulation shows that the creep force factors on both high and low rails in this situation are smaller than their creep force saturation values. This means that at the same condition, the wheel stick-slip process will not happen on the curved track with 420m radius, comparing with that on the track with 240m radius shown in Figure 3 (a).

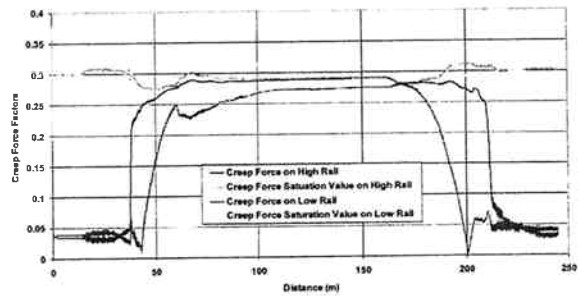

Figure 4. Creep Forces and Saturation Values

4.2 Effect of curved track cant

The simulations are carried out on the 240m radius curved track. The new wheel-rail profile is used. The static and kinetic friction coefficients between wheel and rail are selected to be 0.3 and 0.22. But, the track cant is increased from 65mm to 75mm and 90mm respectively. Simulation results show that at the cant of 75mm, the wheel stick-slip processes on both high and low rails happen in the whole curve section and are quite similar to those at the cant of 65mm in the oscillation frequencies on the high and low rails. However, at the cant of 90mm, in the rear area of curve the wheel stick-slip processes occur as shown in Figure 5 and are also similar to those at the cants of 65mm and 75mm in the oscillation frequencies on the high and low rails.

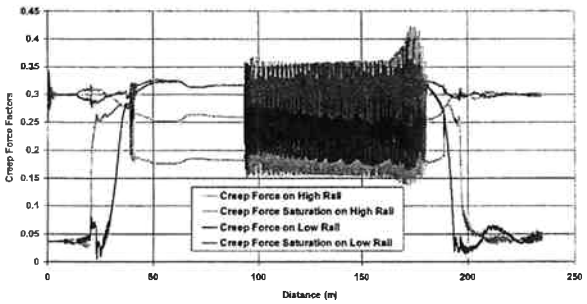

Figure 5. Creep Forces and Saturation Values

4.3 Effect of static friction coefficient between wheel and rail

The simulations are carried out on the 420m radius curved track. The new wheel-rail profile is used. The static friction coefficient between the wheel and the rail is given 0.5, 0.4, 0.3, 0.2 and 0.1 respectively, and the corresponding kinetic friction coefficient is obtained from the interpolation based on the Table 2. Simulation results show that the creep force factors on both high and low rails at the static friction coefficients of 0.5, 0.4 and 0.3 (as shown in Figure 4) are smaller than their creep force saturation values, but are closer if the static friction coefficient is smaller. This means that the potential of wheel stick-slip process is greater at the lower friction situations. It also means that the ability of wheel to overcome the slip is lower as the friction coefficient decreases. However, the wheel stick-slip processes happen when the static friction coefficients are lower (e.g. 0.2 and 0.1). Figure 6 shows the creep force saturation values and the creep force factors on both high and low rails at the static friction coefficient of 0.2.

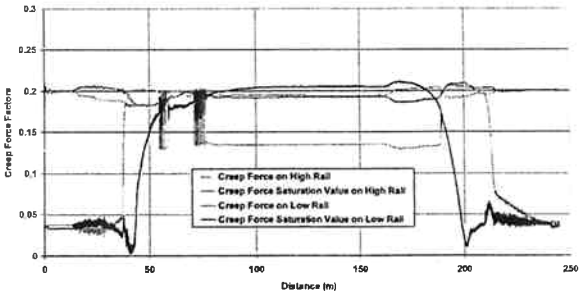

Figure 6. Creep Forces and Saturation Values at Friction Coefficient of 0.2

From Figure 6, it can be seen that the occasional wheel stick-slip processes happen at the some areas between track transition and curve at the situation of friction coefficient of 0.2. The length of larger wheel stick-slip process area is about 7~8 m. It can be also seen that after the second wheel stick-slip process, the wheel keeps slipping on the high rail until it leaves the curve. Although the wheel-rail tangent force on the high rail reduces to the kinetic friction force, the calculated creep force is still larger than the static friction force, causing the wheel to remain slipping on the rail. The creep force on the low rail is just lower than the creep force saturation value, keeping the wheel adhered to the low rail.

4.4 Effect of kinetic friction coefficient between wheel and rail

The simulations are carried out on the 240m radius curved track. The new wheel-rail profile is used. The static friction coefficient between the wheel and the rail is selected to be 0.3 which remains unchanged, but the kinetic friction coefficients are chosen to be 0.22, 0.25, 0.28 and 0.29 respectively. Figure 7 shows the creep force factors and the creep force saturation values on both high and low rails at the kinetic friction coefficient of 0.29.

Figure 3 (a) in the above subsection shows the situation at the kinetic friction coefficient of 0.22. From the simulations shown in Figure 3 (a) and Figure 7, it can be seen that as the kinetic friction coefficient significantly changes the length and magnitude of wheel stick-slip process on the curve.

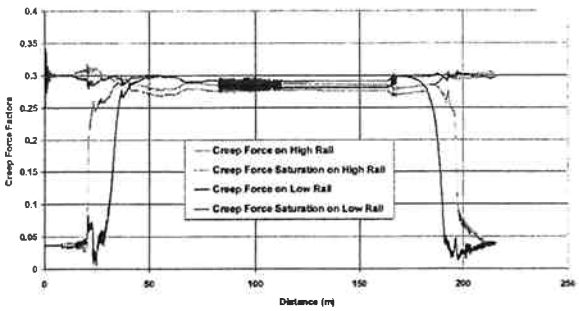

Figure 7. Creep Forces and Saturation Values at Kinetic Friction Coefficient of 0.29

4.5 Effect of wheel-rail profile

The simulation is still carried out on the 240m radius curved track with the cant of 65 mm. Wagon speed is 50 km/h. The static and kinetic friction coefficients between wheel and rail are selected to be 0.3 and 0.22. However, the worn wheel-rail profile is used, and the radius of curvature of wheel profile at the contact point is shown in Figure 8. The simulation results - the creep forces and the creep force saturation values on the leading wheelset on both high and low rails are shown in Figure 9.

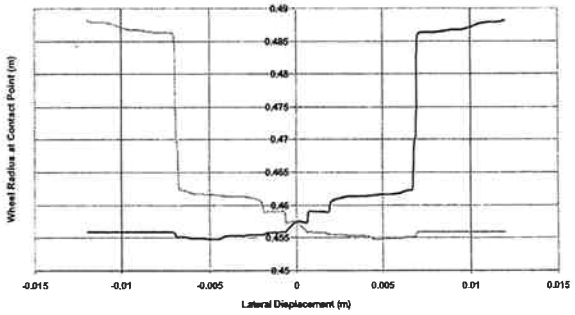

Figure 8. Radius of Curvature of Worn Wheel Profile

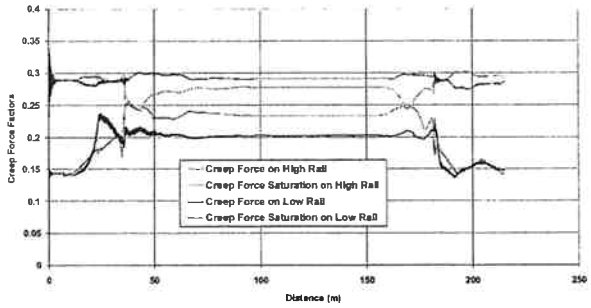

Figure 9. Creep Forces and Saturation Values

The simulation shows that all wheelsets do not have the flange contact during the curving when the worn wheel-rail profile is used. From Figure 9, it can be seen that the creep forces on both high and low rails are lower than the creep force saturation values and the wheel stick-slip process will not happen.

5. Conclusions

The development of the detailed nonlinear wagon-track system model described is necessary for the investigation of rail corrugation initiation. The actual performance of wheel stick-slip process during curving has been simulated. Specifically, the mutual influence between wheelsets, bogies and sleeper spacing could be fully accounted and any possible parameters affecting the rail corrugations could be analysed through such modelling.

The track curvature significantly influences the rail corrugation formations. Generally, the tighter curve can produce the higher creepage between wheel and rail, which overcomes the wheel-rail interface's ability to accommodate it, leading to wheel stick-slip process. The track cant seems to have less influence on the formation of rail corrugations when an intensive wheel stick-slip process is already occurring on the curved track.

The friction characterises between wheel and rail significantly influences the formation of rail corrugations. The low static friction makes the creepage easily to overcome the wheel-rail interface's ability to accommodate it, leading to wheel stick-slip process. Further, the low kinetic friction coefficient intensifies the wheel stick-slip process. The wheel and rail profiles also significantly affect the rail corrugation formations. Generally, the worn wheel profile could easily go through the curved track due to the higher conicity, even without wheel flange contact, reducing the chance for wheel stick-slip process due to the lower creepage between wheel and rail. Generally, the wheel stick-slip process on the high rail oscillates at the basic frequency, which is found to be close to the sleeper-passing frequency and approximately one-third of wheelset torsional frequency. The dominant frequency of wheel stick-slip process on the low rail is double the basic frequency. The components of the triple and four-fold frequencies also appear.

REFERENCES

[1]. Grassie, S. L. and Kalousek, J., 1993. Rail corrugation: characteristics, causes and treatments. Proc Instn Mech Engrs, Vol. 207, 57-68.

[2]. Gòmez, I. and Vadillo, E. G., 2001. An analytical approach to study a special case of booted sleeper track rail corrugation. Wear, Vol 251, 916-924.

[3]. Gòmez, I. and Vadillo, E. G., 2003. A linear model to explain short pitch corrugation on rails. Wear, Vol 255, 1127-1142.

[4]. Ahlbeck, D. R. and Daniels, L. E., 1991. Investigation of rail corrugations on Baltimore Metro. Wear, Vol. 144, 197-210.

[5]. Valdivia, A. R., 1987. A linear dynamic wear model to explain the initiating mechanism of corrugation. Proc. of 10th IAVSD-Symposium, 493-496.

[6]. Hempelmann, K., Grob-Thebing, A. and Kik, W. 2000. Assessment of corrugation growth and derivation of maintenance measures by simulation using SFE AKUSRAIL. Proc of 5th ADAMS / Rail Users' Conference

[7]. Knothe, K. and Ripke, B., 1989. The effects of the parameters of wheelset, track and running conditions on the growth of rail corrugation. Proc. of 11th IAVSD-Symposium, 345-356.

[8]. Tassilly, E. and Vincent, N., 1991. Rail corrugation: analytical model and field tests. Wear, Vol. 144, 163-178.

[9]. Hays, W. F. and Tucker, H. G., 1991. Wheelset-track resonance as a possible source of corrugation wear. Wear, Vol. 144, 211-226.

[10]. Igeland, A., 1996. Railhead corrugation growth explained by dynamic interaction between track and bogie wheelset. Proc Instn Mech Engrs, Vol. 210, 11-20.

[11]. Liu, Q. Y., Zhang, B. and Zhou, Z. R., 2003. An experimental study of rail corrugation. Wear, Vol 255, 1121-1126.

[12]. Jin, X., Wen, Z., Wang, K. and Zhang, W., 2004. Effect of scratch on curved rail on initiation and evolution of rail corrugation. Vol. 37, 385-394.

[13]. Hiemsch, M., Nielsen, J. C. O. and Verheijen, E., 2002. Rail Corrugation in the Netherlands – measurements and simulations. Wear, Vol 253, 140-149.

[14]. Andersson, C. and Johansson, A., 2004. Prediction of rail corrugation generated by three-dimensional wheel-rail interaction. Wear, Vol. 257, 423-434.

[15]. Kalousek, J. and Johnson, K. L., 1992. An investigation of short pitch wheel and rail corrugation on the Vancouver mass transit system. Proc Instn Mech Engrs, Vol. 206, 127-135.

[16]. Grassie, S. L., 1996. Short wavelength rail corrugation: field trials and measuring technology. Wear, Vol. 191, 149-160.

[17]. Clark, R. A. and Foster, P., 1983. On the mechanics of rail corrugation formation. Proc. of 8th IAVSD-Symposium, 72-85.

[18]. Suda, Y. and Iguchi, M., 1989. Basic study of corrugation mechanism on rolling contact in order to control rail surfaces. Proc. of 11th IAVSD-Symposium, 566-577.

[19]. Matsumoto, A., Sato Y., Tanimoto, M., and Qi, K., 1996. Study on the formation mechanism of rail corrugation on curved track. Wagon System Dynamics Supplement, Vol. 25, 450-465.

[20]. Matsumoto, A., Sato Y., Ono, H., Tanimoto, M., Oka, Y. and Miyauchi, E., 2002. Formation mechanism and countermeasures of rail corrugation on curved track. Wear, Vol. 253, 178-184.

[21]. Wu, T. X. and Thompson, D. J., 2002. An investigation into rail corrugation due to micro-slip under multiple wheel/rail interactions. ISVR Technical Memorandum No. 887.

[22]. Ishida, M., Moto, T. and Takikawa, M., 2002. The effect of lateral creepage force on rail corrugation on low rail at sharp curves. Wear, Vol 253, 172-177.

[23]. Ishida, M., Akama, M. Kashiwaya, K. and Kapoor, A., 2003. The current status of theory and practice on rail integrity in Japanese railway – rolling contact fatigue and corrugations. Fatigue Fract Engng Mater Struct, Vol 26, 909-919.

[24]. Kalousek, J. and Magel, E., 1999. Noise control at interface of rail, wheel. Railway Track and Structures; August 01, 1999.

[25]. Manbe, K., 2000. A hypothesis on a wavelength fixing mechanism of rail corrugation. Proc Instn Mech Engrs, Vol. 214, 21-26.

[26]. Sato, Y., Matsumoto, A. and Knothe, K., 2002. Review on rail corrugation studies. Wear, Vol 253, 130-139.

[27]. Garg, V.K. and Dukkipati, R.V., 1984. Dynamics of railway vehicle systems. Academic Press Canada, ISBN 0-12-275950-8.

[28]. Daniel, W.J.T., 2006. Analysis of rail corrugation in cornering. Will be published in 7th International Conference on Contact Mechanics and Wear of Rail/Wheel Systems (CM2006), Brisbane, Australia, September 24-26, 2006